Journal of Hydrology 529 (2015) 1079–1094

Contents lists available at ScienceDirect

Journal of Hydrology

journal homepage: www.elsevier.com/locate/jhydrol

Determining vertical leakage from the Great Artesian Basin, Australia, through up-scaling field estimates of phreatic evapotranspiration

J.F. Costelloe [a,*], V. Matic [a], A.W. Western [a], J.P. Walker [b], M. Tyler [c]

[a] Department of Infrastructure Engineering, University of Melbourne, Victoria 3010, Australia
[b] Department of Civil Engineering, Monash University, Victoria 3800, Australia
[c] Olympic Dam Operations, BHP Billiton, Roxby Downs, SA 5725, Australia

ARTICLE INFO

Article history:
Received 30 June 2015
Received in revised form 2 September 2015
Accepted 10 September 2015
Available online 24 September 2015
This manuscript was handled by Peter K. Kitanidis, Editor-in-Chief, with the assistance of Adrian Deane Werner, Associate Editor

Keywords:
Phreatic evapotranspiration
Leakage
Remote sensing
Water balance
Field measurements

SUMMARY

Understanding the water balance of large groundwater systems is fundamental for the sustainable management of the resource. The vertical leakage (i.e. discharge to upper aquifers or the unconfined water table) component of the Great Artesian Basin (GAB) is an example of a poorly constrained but large component of the water balance of Australia's largest groundwater resource. Field estimates of phreatic evapotranspiration (ET) were made at discharge zones along the southwestern margin of the GAB using eddy covariance station and micro-lysimeter measurements, and inversion of chloride/isotope soil profile measurements. The field estimates were assigned to three major landforms associated with areas of increasingly higher evaporative discharge and progressively decreasing depths to the water table. These landforms were mapped using remote sensing and digital elevation data, with characteristically higher soil moisture, salt precipitation, and lower surface temperature compared to areas distal to discharge zones. Based on the field measurements, broad ranges of phreatic ET (0.5–10, 10–100 and 100–300 mm y^{-1}) were assigned to the major land-types. The higher phreatic ET discharge zones mapped by supervised classification of satellite data are 8–28% of the total regional vertical leakage component estimated by numerical modelling of the GAB. In comparison, the higher discharge zones estimated by landform mapping are 73–251% of the total vertical leakage component estimated by modelling. The mapped distribution of the high discharge areas has important implications for modelling of the GAB. In the western sub-basin, most of the estimated recharge can be accounted for by phreatic ET in the high discharge zones located around the Basin margins, implying that vertical leakage rates distal to the margins are very low and that discharge may exceed current recharge. In contrast, the results for the eastern sub-basin suggest that vertical leakage rates around the South Australian portion of the Basin margin are low and that more of the vertical leakage component in the eastern sub-basin is occurring distal to the Basin margins. Consequently, the pathways for vertical leakage in the eastern sub-basin are likely to be more complex than for the western sub-basin.

1. Introduction

Understanding the water balance of large groundwater systems is fundamental to the sustainable management of the resource (Famiglietti et al., 2011). Regional artesian groundwater is a vital water supply for anthropogenic uses in many arid and semi-arid areas (Habermehl, 1980; Danielopol et al., 2003), in addition to supplying water to ecologically and culturally important surface springs (Mudd, 2000; Fensham and Price, 2004; Harvey et al., 2007). Increasing water demand worldwide has placed a number of groundwater systems under stress (Wada et al., 2010; Famiglietti, 2014). Examples of groundwater depletion are both historical (e.g. Great Artesian Basin of Australia; Habermehl, 1980) and current (e.g. Central Valley of California, Famiglietti et al., 2011), and pose significant risks to groundwater dependent ecosystems (e.g. Patten et al., 2008) and agricultural and other supply (e.g. Famiglietti et al., 2011). The concept of 'sustainable yield' (Bredehoeft et al., 1982; Kalf and Woolley, 2005) in groundwater management requires an understanding of the different recharge and discharge components of the water balance and not just monitoring of groundwater levels.

Measurements of many major components of the water balance of groundwater systems pose considerable challenges and are thus frequently estimated through modelling (Brunner et al., 2012). A shortcoming of the modelling approach is that with insufficient

* Corresponding author. Tel.: +61 3 8344 7238; fax: +61 3 8344 6215.
E-mail address: jcost@unimelb.edu.au (J.F. Costelloe).

http://dx.doi.org/10.1016/j.jhydrol.2015.09.026
0022-1694/

information, the modelled water balance may have high bias and uncertainty (Stisen et al., 2010). This can lead to some of the major fluxes being significantly over-, or under-estimated. For instance, recharge to groundwater (i.e. from rainfall or streamflow percolation) may be over-estimated if other sources of inflow (e.g. leakage from underlying basins) are not well constrained by observed data. Similarly, on the outflow side of the water balance ledger, most of the uncertainty from having inadequate information on all inflow and outflow processes could be assigned to vertical leakage (i.e. discharge to upper aquifers or the unconfined water table due to artesian piezometric heads) (Welsh, 2006). The collection of field data to measure a previously unconstrained, major component of the water balance allows greater confidence to be placed on modelling of the resource and its sustainable use (Tyler et al., 1997). Whilst the uncertainty ranges around the measured fluxes are commonly large, they provide an important independent test of both the magnitude and distribution of the fluxes. An example of such an approach is to measure phreatic evapotranspiration (ET) from saline playas in closed basins to determine the major outflow flux from these systems (e.g. Allison and Barnes, 1985; Kampf et al., 2005; Kampf and Tyler, 2006).

For large groundwater systems, remote sensing provides a vital data source and analysis tool for capturing some hydrological processes at the appropriate spatio-temporal scale (Becker, 2006; Brunner et al., 2007). Recent advances in the use of gravity variation data provided by the Gravity Recovery and Climate Experiment (GRACE) satellites has enabled whole of basin estimates of water volume changes (Rodell et al., 2009; van Dijk et al., 2011; Wang et al., 2014). While a powerful technique, the GRACE data do not provide insights into the detailed spatial distribution of recharge and discharge processes. Satellites measuring information in the optical through to microwave spectrum can provide observations at much finer spatial scales than GRACE and hence on recharge and discharge zones of the groundwater system where fluxes are potentially observable at the land surface (Becker, 2006; Leblanc et al., 2007). For example, Hendricks Franssen et al. (2008) used remote sensing to constrain recharge rates indicated by chloride profiles in Botswana, whilst Brunner et al. (2008) used remotely sensed maps of ET to extract the phreatic component in China.

Phreatic ET can form a large part of the water budget of groundwater systems in the arid zone, such as in salt lakes and artesian discharge zones (Habermehl, 1980; Tyler et al., 2006; Sultan et al., 2007). For many closed basins, phreatic evaporation through a salt lake can be the dominant outflow from the system (Allison and Barnes, 1985), but for other large groundwater systems, phreatic ET may form a component of the outflow, in conjunction with spring flow, bore extraction, and flow into other groundwater systems (the latter could include underlying and overlying aquifers and other groundwater basins). Estimating the phreatic ET loss can improve understanding of groundwater processes in these systems, which are typically characterised by low flux rates, and can assist in assessing sustainable extraction from the groundwater basin (Sultan et al., 2007).

The vertical leakage of the Great Artesian Basin (GAB) supplying phreatic ET is an example of a poorly constrained but large component of the water balance of Australia's largest groundwater resource (Habermehl, 1980; Woods, 1990; Welsh, 2000). Steady-state and transient groundwater modelling of the GAB (Welsh, 2000, 2006) indicates that 12–53% of the total discharge from the GAB occurs as vertical leakage. Along the south-western margin of the GAB in South Australia, steady state modelling indicates that vertical leakage accounts for 58% of the discharge in this region. Defining the likely spatial distribution and rates of leakage are critical for reliable modelling of this major basin. Recently, Harrington et al. (2013) used modelling of tracer profiles through the matrix of the main aquitard to estimate a bulk vertical hydraulic conductivity of $<1 \times 10^{-12}$ ms^{-1} that inferred diffuse vertical leakage rates in the order of a few millimetres per ten thousand years. However, around the spring groups occurring along the south-western discharge margin of the GAB (Fig. 1), considerable areas of shallow groundwater and salt precipitation suggest that GAB water supplying the springs also leaks into the unconfined groundwater and is depleted by phreatic ET (Costelloe et al., 2012, 2014). If the phreatic ET is considered to be in balance with the vertical leakage to the shallow water table, then these surface expressions of phreatic ET (e.g. moist soils and salt precipitation) provide a means of mapping zones of high discharge (as phreatic ET). Characteristically, these high discharge zones are dominated by bare soil and so phreatic evaporation through the soil profile will account for most ET. The discharge zones lack deep rooted vegetation, as trees are mostly restricted to stream margins in this region, but they can contain relatively sparse populations of small halophytic shrubs, such as *Halosarcia*, *Frankenia* and chenopods, that will provide some transpiration component to ET. Increased water resource demand, particularly from mining operations, requires improved understanding of natural discharge processes in the GAB (Mudd, 2000). This will lead to improved protection of unique ecosystems (e.g. mound springs, Fensham and Price, 2004) dependent on flow from the GAB and greater security of supply for all users of the GAB resource. This paper reports on the integrated use of field measurements and remote sensing to estimate discharge occurring as phreatic ET along the south-western margin of the GAB in central Australia. The paper argues that the integration of field measurements, with a conceptual model of surface characteristics that can be mapped using remote sensing, allows a robust method for estimating spatially varying, low rates of phreatic ET.

2. The Great Artesian Basin

The Great Artesian Basin is the largest groundwater resource in Australia and one of the largest artesian basins in the world (Habermehl, 1980). It underlies 22% of the Australian continent (Fig. 1) and is the only practical water resource available to mining and pastoral operations throughout much of the arid and semi-arid zone of central and eastern Australia. Most of the utilised water resource of the GAB occurs in the basal Lower Cretaceous and Jurassic aquifers (J-K aquifers), which are typically hydraulically connected and considered as a single aquifer (Habermehl, 1980). The GAB can be divided into an eastern and western sub-basin (Habermehl, 1980, Fig. 1). The much larger eastern sub-basin has groundwater flow from the east to the west, originating from recharge areas on the eastern margin in Queensland (Qld) and New South Wales (NSW). The smaller western sub-basin has its recharge areas along the western margin of the GAB in South Australia (SA) and Northern Territory (NT) with flow patterns from the west to the east. In the area around Lake Eyre, there is a mixing zone with contributions from the eastern and western sub-basins (Herczeg et al., 1991; Costelloe et al., 2012; Love et al., 2013a).

Much of the groundwater flow throughout the GAB is focused towards discharge zones along the south-western margin (Habermehl, 1980), with water discharged by bores, natural springs ("mound springs") and vertical leakage. Due to the large spatial scale of the GAB, only modelling methods have been used to estimate the vertical leakage at a sub-basin scale (Welsh, 2000, 2006). Relatively few field measurements are available to constrain the rate or regional distribution of this vertical leakage, despite modelling suggesting that it comprises up to 53% of the

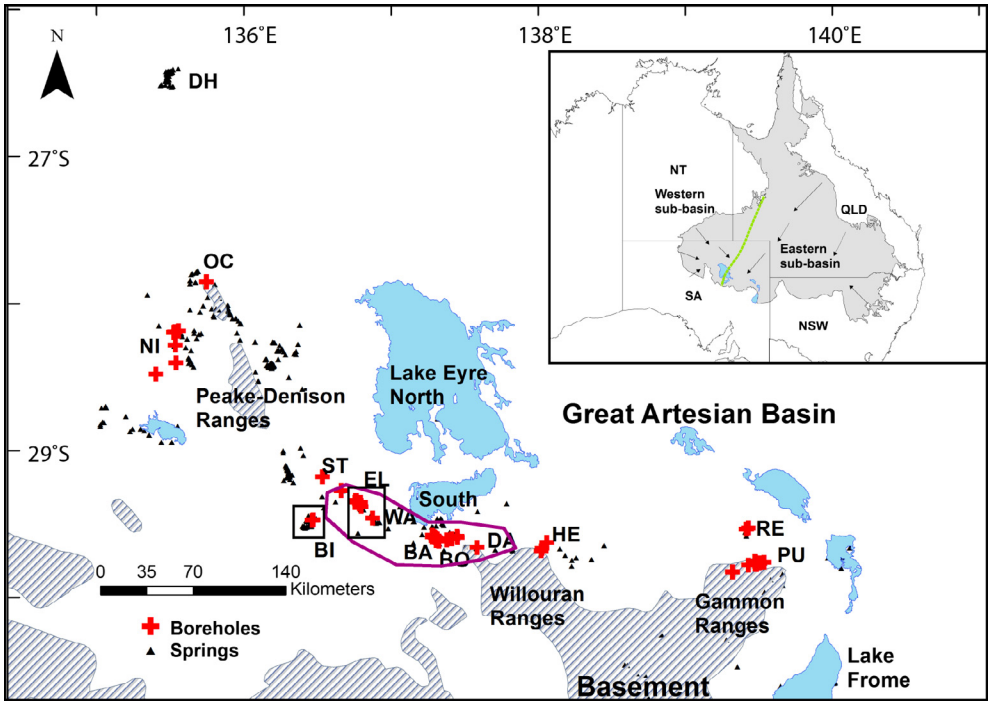

Fig. 1. Location diagram of field areas within the GAB. Outcrop of Proterozoic basement forming the GAB margin is shown by grey-striped polygons. Salt lakes are shown in blue. The discharge areas along the south-western margin of the GAB are approximately shown by the position of artesian springs (triangles). The locations of boreholes drilled for this study are shown as crosses. The two letter codes refer to field sites with data collection. The mixing zone between the Eastern sub-basin and the Western sub-basin is shown within the purple polygon and the locations of areas covered in Fig. 3 are shown as black rectangles. (For interpretation of the references to colour in this figure legend, the reader is referred to the web version of this article.)

total discharge from the GAB; although there have been important advances in recent years (e.g. Harrington et al., 2013; Love et al., 2013b). Rates of phreatic evaporation along part of the south-western GAB margin (near Lake Eyre South) were first analysed by Woods (1990) using soil profile modelling, where rates of 3.0–7.0 mm y^{-1} were estimated. Harrington et al. (2013) found rates of <0.001 mm y^{-1} for diffuse discharge through the aquitard matrix away from the discharge zones represented by the occurrence of spring groups. Conceptually, some artesian water could be harvested that would otherwise be discharged by upwards leakage into the less important unconfined water table (Sultan et al., 2007). However to be sustainable, such harvesting would require knowledge of the rates and spatial distribution of the upward leaking discharge.

This study gathered data over much of the south-western margin of the GAB (Fig. 1). Field data were collected from the Public House Springs (PU, Fig. 1) on the northern tip of the Gammon Ranges, through an arc moving west and north to discharge areas at the northern tip of the Peake-Denison Ranges (OC, Fig. 1). Remote sensing data were analysed over this area and also extended to cover the Dalhousie Springs complex (DH, Fig. 1), approximately 130 km north of the field area. Discharge zones around the Lake Frome spring super group, south-east of Public House Springs, were not included in the study area. The field area coincides with the arid core of Australia with typical conditions measured at Marree (Station 017031, www.bom.gov.au, near location HE in Fig. 1) having a mean annual rainfall of 162 mm (range 39–409 mm y^{-1}) and a mean annual areal potential evapotranspiration (APET) rate of 1300 mm. The mean monthly APET rate exceeds the mean monthly rainfall in all months and the mean number of rain-days with $\geqslant$25 mm of daily rainfall per year is 1.2. These climatic conditions favour high rates of ET and only rare rainfall events that are likely to lead to significant meteoric recharge to the unconfined groundwater.

3. Methods

3.1. Field measurements

Field estimates of evaporation and evapotranspiration were measured using small foot-print (order ~300 m) and point-based field techniques; eddy covariance stations, micro-lysimeters and chloride/isotope soil profile modelling. These estimates were assumed to represent phreatic ET and this is considered further in the discussion of the results. Data were collected from 12 locations along the south-western margin of the GAB (Fig. 1) during four field trips in the period 2007–2009 (June–July 2007, November 2007, November 2008, May 2009).

A simple microlysimeter technique (Boast and Robinson, 1982) for estimating bare soil evaporation has been used by many studies in both temperate and arid climates (Plauborg, 1995; Tyler et al., 1997). This technique provides a point measurement of evaporation and relies on few assumptions. Microlysimeters were installed in areas with both salt precipitation at the surface and moist soils, indicating probable high rates of phreatic ET. The microlysimeters consisted of a 0.3 m length of 0.09 m diameter PVC pipe (or 0.1 m diameter steel pipe) hammered into the surface to obtain a soil core. The soil core was retrieved and the bottom of the pipe capped, prior to installation into another PVC pipe of slightly larger diameter, and both inserted into the soil from where the previous pipe was removed. Both pipes were installed flush with the ground surface, taking care that disturbance of the salt/surface crust of the soil core and surrounding ground surface was minimised. The microlysimeters were then weighed daily at approximately the same time of day over a 4–7 day period. The daily weight loss was converted to a volumetric water loss and expressed as an evaporative loss in mm using the cross-sectional area of the microlysimeter. The mean evaporation loss was determined as the mean of the cumulative loss and also as the gradient of a line

of best fit through the data. Selected microlysimeter cores were also subjected to further evaporation treatment under laboratory conditions using a heat lamp to drive evaporation fluxes over longer periods of time (further described in Costelloe et al., 2009).

An eddy covariance station was also installed in the areas having moist soils and salt precipitation at the surface to provide an estimate of spatially averaged net ET fluxes above the ground surface. This technique has been applied to salt lake environments to estimate phreatic ET (Kampf et al., 2005; Kampf and Tyler, 2006). The installation used a three-dimensional sonic anemometer (CSAT3, Campbell Scientific) and a gas analyser (LICOR 7500) to measure rates of actual evapotranspiration above the ground surface of the saline discharge zones. The atmospheric sensors were installed approximately 2.5 m above the ground surface and were operated at 10 Hz, while averaging fluxes over 30 min intervals. The 2.5 m height of the instrumentation gave an upwind fetch (or area providing the ET flux) in the region of about 250–300 m radius. Radiation (four-way net radiometer, Kipp and Zonen) and soil heat (two soil heat flux plates) flux measurements were also made to allow for calculation of energy balance closure.

Shallow cored auger holes (<6 m depth) were drilled within 1 km of artesian springs that were surrounded by areas of obvious phreatic ET (i.e. salt precipitation at the surface and moist soils). The locations ranged from areas of moist salt flats, to surrounding slightly higher landscapes with dry soils and no sign of salt precipitation at the surface. Core samples were collected and chloride concentration, oxygen isotope ($\delta^{18}O$) values and gravimetric soil water content (θ) of soil water samples were analysed at the Land and Water Laboratory of the Commonwealth Scientific and Industrial Research Organization (CSIRO) in Adelaide, Australia. These values were used to estimate long term flux rates through the unsaturated sections of the soil profile, using a steady state advection–diffusion model (Barnes and Allison, 1983; Costelloe et al., 2014). In total, soil profile samples were obtained from 28 shallow boreholes in a variety of locations. Typically, the first 0.5 m of the core profile from the surface was continuously sampled at 0.1 m intervals (usually 0.05 m interval for the surface sample). At greater depths, 1–2 samples of 0.1 m length were selected over each 0.5 m of cored soil profile. Further details of the soil profile method are found in Costelloe et al. (2014).

To assist the interpretation of remotely sensed images of the field area (Section 3.3), mapping was carried out along transects designed to cover the major regolith materials and landforms in each study area, with a particular focus on regolith materials related to discharge processes (i.e. presence of surface salt, soil moisture, vegetation). Differential Global Positioning System (DGPS) data were collected at each sample location to collect the latitude, longitude and elevation in units of the Australian Height Datum (AHD) (m). These data provided high resolution information for characterising the terrain and topographic relief found within each landform. Soil moisture was measured either by volumetric soil samples or using a hand held conductance probe (Hydraprobe, Merlin et al., 2007). Visual estimates were made of salt precipitation, surface lag material, and vegetation type and density, at locations along each transect.

Two of the techniques (microlysimeters and soil profile modelling) provide point measurements of only the bare soil evaporation component of the phreatic ET, while the third method (eddy covariance) measures spatially averaged total evapotranspiration. No specific transpiration rates were measured in this project but bare soil evaporation is likely to dominate phreatic ET in the sparsely vegetated discharge zones of the field area. The field estimates of phreatic ET were assigned to three major land-types associated with areas of increasingly higher ET rates (see Section 3.2). These land-types were mapped using remote sensing, digital elevation data and field observations.

3.2. Landscape conceptual framework

A conceptual framework was used to classify areas of high phreatic ET into relatively homogenous areas based on surface characteristics (Fig. 2). Areas with shallow water tables (typically <1 m deep) are considered to allow water to rise through capillary action to the near surface (i.e. within 0.05 m of the surface) in clay and silt based soils, and are classified as the Liquid Transport Zone (LTZ). This zone is considered to represent the highest phreatic ET rates and is characterised by moist soils throughout the profile, significant salt precipitation at the surface, and relatively low surface temperatures (see representative LTZ chloride concentration and soil moisture profile in Fig. 2). As the depth to the water table increases, the near-surface soil moisture decreases and the evaporation front occurs below the ground surface with water transport in both liquid and vapour phases in the near surface environment. Such areas are classified as the Mixed Transport Zone (MTZ). As a result, these discharge areas are characterised by drier soils, with less salt precipitation at the surface (see representative MTZ profile in Fig. 2) and a lower temperature contrast with the surrounding dry ground. With increasing depth to groundwater (i.e. water table depths approximately >3–4 m) the evaporation front occurs >0.1 m below the ground surface and vapour transport dominates at the surface (classified as the Vapour Transport Zone (VTZ)). The VTZ no longer has any observable salt precipitation, contains dry surface soils (see representative VTZ profile in Fig. 2) and has practically no temperature contrast with the surrounding dry ground. As a result of the lack of surface characteristics, the outer extent of the VTZ cannot be directly mapped in the field or by remote sensing. As the depth to groundwater increases beyond some threshold, phreatic ET is considered to be effectively zero and this is termed the Zero Discharge Zone (ZDZ). This study has, therefore, focused on defining the extent of, and phreatic ET rates from, the LTZ and MTZ. Field mapping indicated that a fourth zone occasionally occurs around the GAB discharge areas (termed the carbonate zone), that comprises areas of flat-lying massive carbonate layers that may be related to carbonate precipitation observed around GAB artesian springs (Keppel et al., 2011). These layers typically occur at a particular local topographic level, can be 1–2 m thick, and may extend under alluvial–colluvial cover away from the spring groups and high discharge zones.

Landform mapping was applied to the field areas to provide an interpretative measure of the extent of the discharge zones. This was done by visual interpretation of a variety of data sets. Landsat TM images were used to create base maps from which the major landform units present in the study areas were mapped. At some sites, high spatial resolution digital aerial photographs and Quickbird satellite images were available and these were used to complement the landform mapping using Landsat. In addition, the Shuttle Radar Terrain Model (SRTM) 3 arc-sec DEM product was used in the mapping and interpretation of landforms. The discharge zones generally corresponded with topographically low areas that could be identified using the DEM data. Transects and associated field observations were used to characterise the landforms' structure, surface materials and boundaries. These field verified maps were then used to quantitatively estimate the GAB discharge zones across the south-western margin of the GAB, and also used to evaluate the supervised classification of the discharge zones using satellite data (Section 3.3).

3.3. Remote sensing of discharge zones

Due to its suitable spatial and spectral resolution in mapping phreatic ET scale processes, two Landsat indices were used for classification of the zones of higher phreatic ET with distinctive surface characteristics (LTZ and MTZ). The Modified Normalized

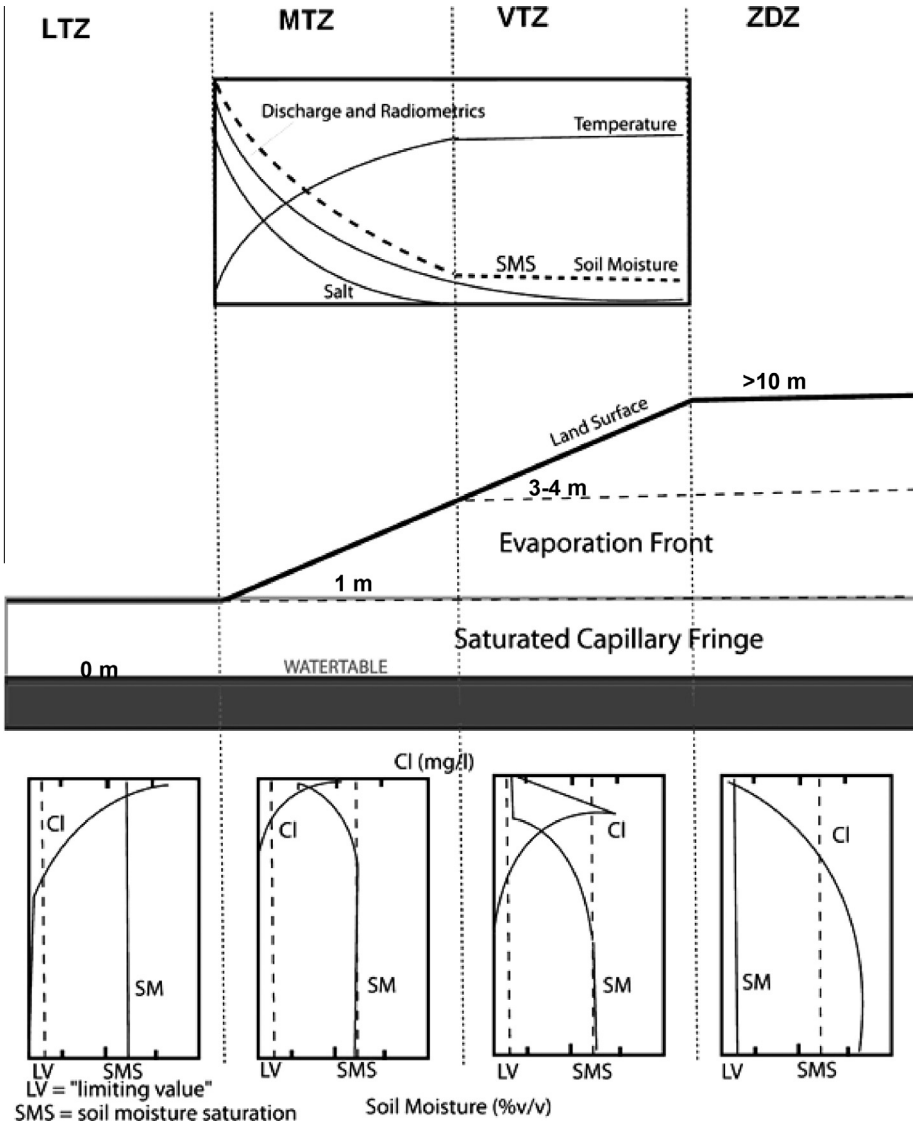

Fig. 2. Conceptual framework for linking zones with distinctive surface (e.g. soil moisture, surface salt precipitation) and sub-surface (e.g. chloride (Cl) concentrations, soil moisture (SM)) characteristics to depth to water table and phreatic ET fluxes. LTZ – Liquid Transport Zone, MTZ – Mixed Transport Zone, VTZ – Vapour Transport Zone, ZDZ – Zero Discharge Zone. Indicative threshold depths for each zone, relative to the position of the water table (0 m), and characteristic sub-surface Cl and SM profiles, are shown for each zone.

Difference Wetness Index (MNDWI) (Eq. (1)) highlights the short wave infrared soil moisture absorption feature (Xu, 2006) and was used to delineate areas of high soil moisture that define the LTZ. The Salinity Index (SI) (Eq. (2)) has been used to map areas with salt precipitation at the land surface (Tripathi et al., 1997) by making use of the high albedo of salt crusts. The MTZ was mapped using the SI where the MNDWI fell below threshold values defining the LTZ. Only these indices were used in the mapping of the high discharge zones based on the supervised classification of Landsat 5 images from 2004 to 2010.

$$\mathrm{MNDWI} = (\mathrm{Green} - \mathrm{MIR})/(\mathrm{Green} + \mathrm{MIR}) \quad (1)$$

$$\mathrm{SI} = (\mathrm{Green} \times \mathrm{Red})^{0.5} \quad (2)$$

Ground truth data were collected along field transects (Section 3.1) and each point was characterised as either wet or dry (based on the real component of the dielectric constant measured by a handheld theta probe), and whether or not it featured surface salt precipitation by visual assessment. Each point was then classified as LTZ, MTZ or other, based on the salt and soil moisture classification. For the Landsat image Path 99/Row 80, approximately 1000 points were classified from transects located around six artesian spring groups and used in a calibration exercise. The pixel value of each index was extracted for each sample location to input into an error matrix/accuracy assessment (Congalton, 1991). The user and producer accuracies (*ibid.*) for both classes were then calculated and evaluated for different threshold values using all ground truth points. A second approach was also used for evaluation of the accuracy of supervised classification using varying threshold index values by comparing the results against the landform mapping. As the index value is relaxed beyond an optimum value, the classified area should increase, extending outwards from the discharge area and creating 'false positives'. The second approach is illustrated for the MNDWI index at two of the calibration sites (BI, WA in Fig. 1) using two Landsat scenes from September 2003 and February 2004 (Fig. 3).

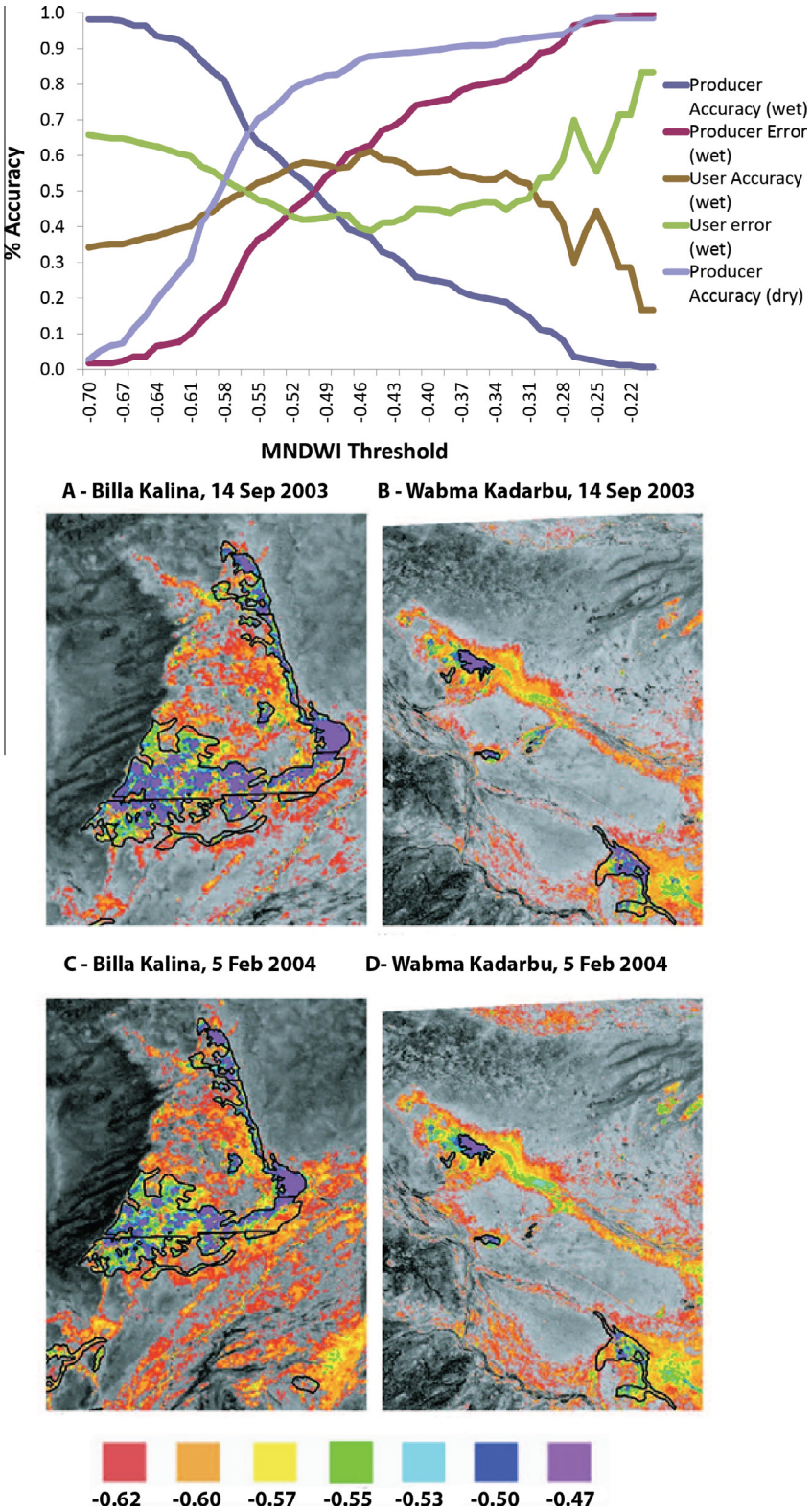

Fig. 3. Examples of calibration of MNDWI index against landform mapping (black polygons) for supervised classification of the LTZ at Billa Kalina and Wabma Kadarbu (BI, WA in Fig. 1, respectively). Landsat images (99, 80) from 14th September 2003 and 5th February 2004 are used in the supervised classification. Approximate thresholds for where false positives occur outside of landform mapping of the LTZ were −0.57 (A), −0.55 (B) and −0.52 (C and D). At MNDWI values above these thresholds the classified areas occurred within the landform mapping of probable LTZ, while values increasingly below these thresholds generated increasing areas of false positives.

4. Results

The field results for each measurement technique (microlysimeters, eddy covariance, soil profile modelling) are presented in terms of the discharge zones (LTZ, MTZ, VTZ) identified by the conceptual model developed for the remote sensing analysis (Table 1). All results showed wide ranges, but a consistent decrease in discharge rates moving between zones and coinciding with an increase in the

Table 1
Range of field measured phreatic ET for the different zones. The mean of field measurements for each method and zone are given in brackets, except for soil profile modelling. For the previous studies, the approximate depth to groundwater is shown in brackets in the Comments column. More detailed information on site measurement results are provided in the Supplementary Table.

Zone	LTZ	MTZ	VTZ	Comments
Water table depth (m)	0.3–0.9	1.3 to >3.5	>3.0	
Microlysimeters (mm y^{-1})	96–542 (279)	41–449 (145)	–	Not applied in VTZ
Eddy covariance (mm y^{-1})	44–455 (175)	32–157 (78)	–	Not applied in VTZ
Soil profile modelling (mm y^{-1})	2–456	0.2–86	<0.1–17	
Final range (mm y^{-1})	100–300	10–100	0.5–10	
Previous studies	(mm y^{-1})	(mm y^{-1})	(mm y^{-1})	
Woods (1990)		3–7	3–7	Outer margins of GAB spring zones
Allison and Barnes (1985)	90–230			Saline playa (<1 m)
Tyler et al. (1997)	88–104	88–104		Playa (0.9–2.5 m). Soils near saturation
Sanderson and Cooper (2008)		163–449		Vegetated playa (1.5–1.7 m)
Kampf et al. (2005)	37–402			Saline playa (0.2–0.9 m), salt crust
Kampf et al. (2005)	146–1022			Saline playa (0.2–0.9 m), vegetated
Brunner et al. (2008)	200–600	200–600		Arid basin (0.8–2.0 m)
Shanafield et al. (2015)		0.1–300		Saline playa – claypan (1–3 m)

depth to the water table. The remote sensing techniques (supervised classification and landform mapping) were only able to map the high discharge zones (LTZ, MTZ and carbonate) and could not constrain the outer extent of the VTZ around these areas. No definitive measurements were available from the carbonate zone due to the difficulty in drilling soil profiles through the massive carbonate layer. However, the very low soil moisture in the near surface of the carbonate zone indicates that it would share a similar range in discharge as the VTZ but with a decreased upper limit.

4.1. Field measurements of discharge – liquid transport zone

Field estimates of bare soil evaporation in the LTZ using microlysimeters ranged from 96 to 542 mm y^{-1} with a mean of 279 mm y^{-1} and standard deviation of 112 mm y^{-1}. The results include estimates using cumulative weight losses and linear best fits (see Fig. 4) from 20 microlysimeters measured over periods of 4–6 days. These estimates are significantly below the mean annual areal potential evapotranspiration rates for the region (1300–1400 mm, Australian Bureau of Meteorology) and probably reflect the influence of soil characteristics, as well as thin salt crusts and high soil water salinities, in decreasing evaporation rates.

The eddy covariance data were collected at three LTZ sites (EL, NI, OC, Fig. 1), but on all occasions results were affected by rainfall within a few days of the measurements. The daily measurements were converted to annual estimates that ranged from 44 to 455 mm y^{-1} with a mean of 175 mm y^{-1} and standard deviation of 131 mm y^{-1}. Half-hourly latent and sensible heat energy data from the LTZ Elizabeth Springs (EL) site (Fig. 5) show that in days following rainfall contribution, the sensible energy flux was similar, or smaller than, the latent energy flux. Data from MTZ sites not affected by rainfall show that latent energy fluxes were much smaller than sensible energy fluxes and thus taken as representative of phreatic ET rates (see HE site in Fig. 5 and Section 4.2). The least rainfall-affected discharge rates measured by the eddy covariance stations in the LTZ were in the range of 54–151 mm y^{-1} but may also integrate lower rates derived from areas of MTZ (and perhaps even VTZ) in the upwind fetch of the stations. The correlation between the sensible and latent heat flux terms (H + LE) with the difference between the net radiation and soil heat flux (R_n-G) provides a measure of the closure of the surface energy balance at the site. For both the LTZ and MTZ, the range in slope values of 0.46–0.63 indicates that the H + LE term is significantly underestimated compared to the R_n-G term (i.e. on average, the H + LE term is 46–63% of the R_n-G term). This large underestimation may reflect the differences in the spatial scale at which the two sets of measurements were collected. The net radiation and soil heat flux data represent conditions directly beneath the radiometer and around the soil heat flux plates, respectively. The area of influence around these instruments is on the order of a few square metres. In contrast, the sensible and latent heat energy fluxes were measured by the eddy covariance instrument and represent an area of influence of possibly several thousand square metres. Thus, the larger area measured by the sensible and latent heat energy data probably incorporates lower discharge areas than the salt-crusted location where the net radiation and soil heat flux data were collected. However, the lack of closure of the energy balance does imply that the sensible and latent heat fluxes are not being overestimated and so the evapotranspiration determined by this method is likely to represent a minimum rate for the area.

Five soil profiles were collected in the LTZ and were characterised by having shallow (<1 m below ground level (BGL)), moderate salinity (<12,000 mg L^{-1} total dissolved solids (TDS)) unconfined groundwater. The overall range of modelled discharges for these soil profiles was 2–456 mm y^{-1} and this large range was driven by model uncertainties arising from the position of the evaporation front and salinity of groundwater (Costelloe et al., 2014) within individual profiles. Modelled profiles from the LTZ at Elizabeth Springs are shown in Fig. 6 (top) and show that model fits are typically noisy for the shallow profiles in the LTZ and very sensitive to the placement of the evaporation front either in, or below, dry upper soil layers. All of the profiles showed large ranges in modelled evaporation fluxes, with the smallest range being 10–56 mm y^{-1} and the largest being 14–456 mm y^{-1}.

4.2. Field measurements of discharge – mixed transport zone

Field estimates of bare soil evaporation in the MTZ using microlysimeters ranged from 41 to 449 mm y^{-1} with a mean of 145 mm y^{-1} and standard deviation of 93 mm y^{-1} (see examples in Fig. 4). Excluding microlysimeter data collected after rainfall in May 2009 (OC site) reduces the mean to 134 mm y^{-1} with a standard deviation of 102 mm y^{-1}. Selected cores from the MTZ were also measured over significantly longer periods of time (e.g. 15–30 days) under laboratory conditions and compared to the field sample results. The laboratory-measured cores showed non-linear weight loss behaviour that decreased with time as the core dried (Fig. 4). The laboratory analyses of loss rates supported the field results and were in the range of 60–480 mm y^{-1} with short-term mean rates of 97–333 mm y^{-1} (i.e. over periods or 5–30 days, depending on which part of the non-linear evaporative curve is used). In general, the microlysimeter data show poor ranked

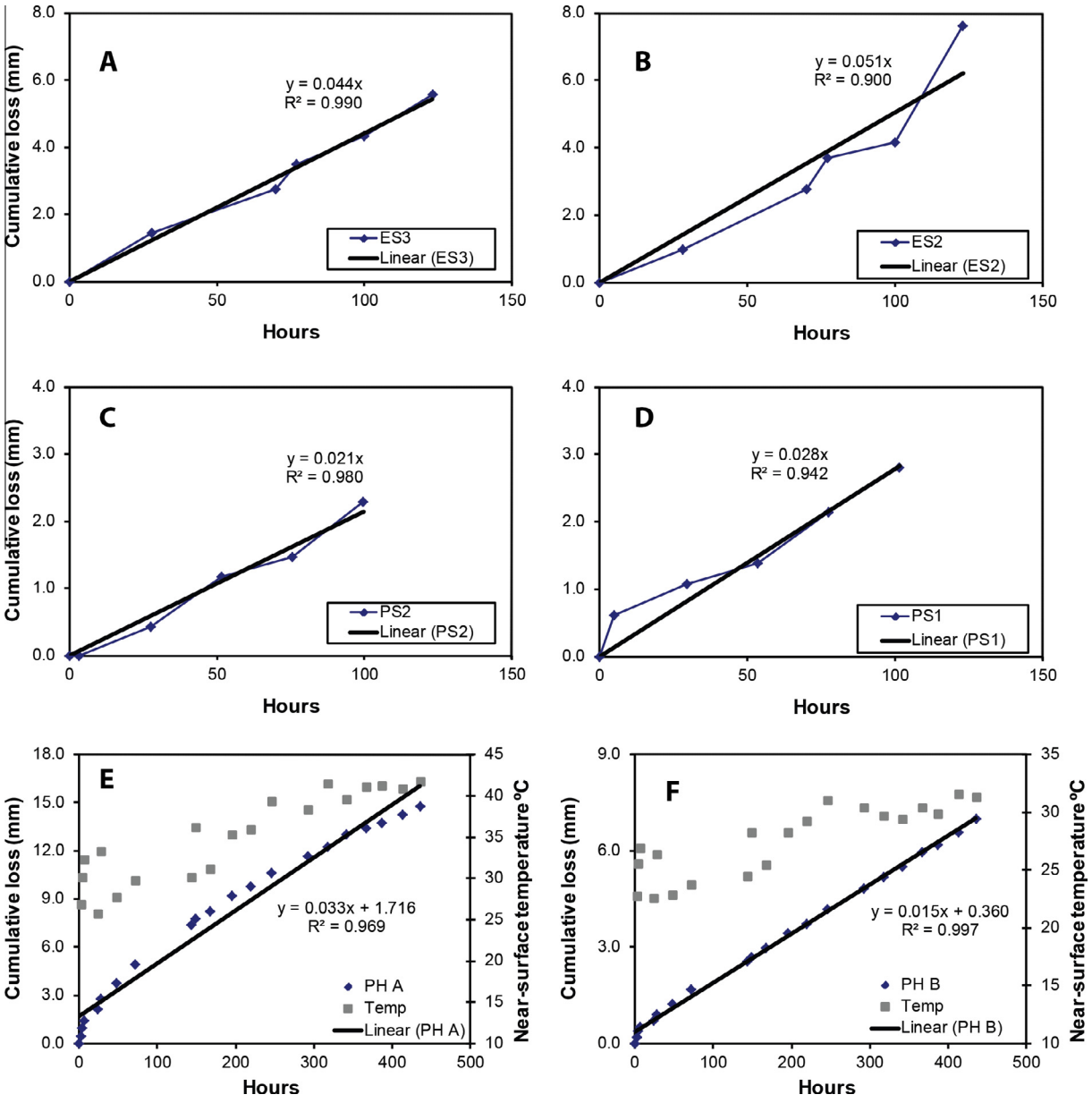

Fig. 4. Representative microlysimeter results from the LTZ at Elizabeth Springs (EL in Fig. 1) during November 2007 (A and B); from the MTZ at Public House Springs (PU in Fig. 1) in July 2007 (C and D); and from laboratory controlled loss rates measured from cores collected at Public House Springs in November 2008 (E and F).

correlations between evaporation rates and relative height differences within a site, and also with estimated depths to groundwater between sites. This may reflect local scale variation in soil water content driven by differences in soil type and uncertainties in the position of the water table.

Eddy covariance data were collected from MTZ sites at four locations (HE-June 2007, PU-July 2007, November 2008, RE-July 2007) and results from HE are shown as an example of MTZ eddy covariance data in Fig. 5. Excluding the rainfall-affected Public House Springs (PU) results from November 2008, the eddy covariance discharge rates had a range of 32–157 mm y^{-1} with a mean of 78 mm y^{-1} and standard deviation of 42 mm y^{-1}. The rain-affected eddy covariance discharge rates from Public House Springs had a range of 246–401 mm y^{-1}. The non-rain affected values were all measured in the winter trip of June–July 2007 and so probably do not represent the highest short-term rates that could be measured from the MTZ. However, it is possible that some areas of LTZ, open spring pools or night-time condensation, could be contributing to the higher values measured in the MTZ, that are very similar to the eddy covariance range measured in the LTZ.

Eleven soil profiles were collected in the MTZ showing approximately steady-state evaporation characteristics. These profiles occurred in areas with water table depths of 1.7 m to >4.5 m BGL and high groundwater salinity (13,000–192,000 mg L^{-1}, mean 78,000 mg L^{-1} TDS). These profiles also showed evaporation fronts occurring between the surface and 0.4 m depth, with a mean depth of 0.14 m, indicating that most evaporation was occurring in the sub-surface, thus limiting soil moisture and salt precipitation at the surface. Soil profile modelling results from the MTZ showed a range of 0.2–86 mm y^{-1} and this range was generally less than estimated from the LTZ soil profile modelling results. Results representative of the MTZ are shown in Fig. 6b for a soil profile from Strangways Springs (ST) where the water table was 1.7–2.2 m below ground surface. Similar to the LTZ, the lower end of the MTZ results were heavily influenced by dry soil samples at the top of the profile being incorporated into the modelling and thus

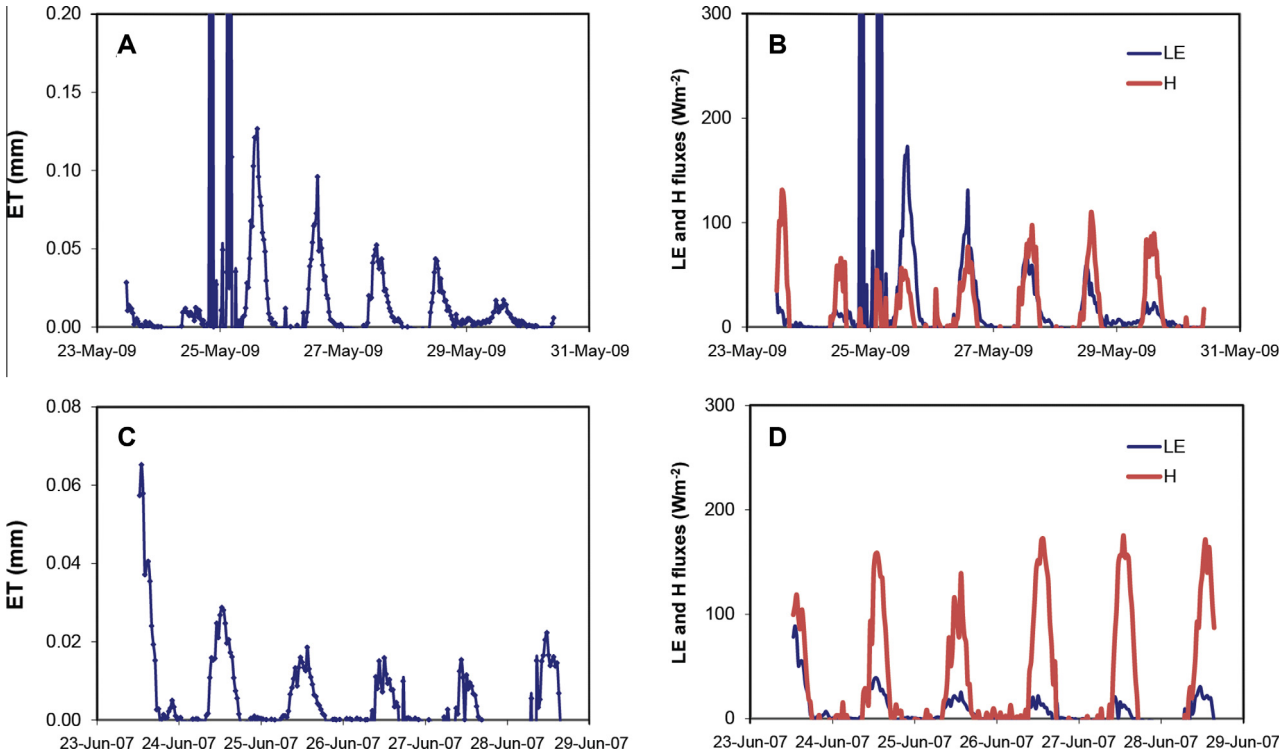

Fig. 5. (A and B) Eddy covariance results from Elizabeth Springs installation (EL in Fig. 1), May 2009 (39% LTZ, 61% MTZ within a 300 m radius of installation from landform mapping). (C and D) Eddy covariance results from Hergott Spring (HE in Fig. 1), June 2007 (6% LTZ, 62% MTZ, 31% VTZ within a 300 m radius of installation from landform mapping). The left hand side plots (A and C) show the half hourly ET (converted from latent energy) rates and the right hand plots (B and D) show the half-hourly latent and sensible energy flux rates. Approximately 3.0 mm of rainfall fell at Elizabeth Springs on the night of the 24/05/09 but there was no further rain for the remainder of the sampling period. The Hergott Springs site experienced 0.9 mm of rainfall on the night of 22/06/07.

these lower results probably underestimate the long-term evaporative discharge rates. The modelling was also sensitive to the groundwater concentration not being in equilibrium with the deeper sections of the soil profile (e.g. Fig. 6b).

4.3. Field measurements of discharge – vapour transport zone

No microlysimeters were installed in the VTZ zone due to the difficulty in obtaining a soil core in dry sediments, and eddy covariance stations were not located in the VTZ at any of the field sites either. Phreatic evaporation estimates for this zone relied on the soil profile modelling. Seven boreholes were identified as occurring in the VTZ as their evaporation fronts occurred between 0.20 and 0.75 m depth, being typically deeper than for profiles occurring in the MTZ. In addition, the gravimetric water contents of the uppermost 0.1 m of the profiles were low (0.023–0.034 g/g) with the exception of those drilled within a week of rainfall (PU9, EL5, EL6, 0.072–0.102 g/g), and no salt precipitates were visible on the ground surface. The unconfined water table was not intersected in any of the VTZ boreholes, with the water table typically >5 m deep at least. The results from the soil profile modelling showed a wide range (<0.1–17.4 mm y^{-1}) with most results being consistently lower than the results from the MTZ and LTZ. An example of a VTZ soil profile is shown from Elizabeth Springs (EL) in Fig. 6c (water table >5 m deep) where the chloride and $\delta^{18}O$ tracers had not yet approached a concentration that asymptotes towards the concentration of the unknown groundwater reservoir.

4.4. Mapping of discharge areas

The results of the mapping of the GAB discharge areas using supervised classification and landform mapping are shown in Table 2 and Fig. 7. The calibration of the MNDWI values against field point data for mapping the LTZ indicated that threshold values for identifying 'wet' pixels (i.e. LTZ) ranged from −0.51 (conservative, few false positives) to −0.58 (increase in false negatives). Comparison of different thresholds against landform mapping of the LTZ at the calibration sites (BI and WA, Fig. 3) indicate that a threshold of −0.51 for the MDNWI does not result in obvious false positives. Furthermore, it appears that even slightly relaxing the threshold to −0.53 could be used without false positives in most images (i.e. the yellow[1] to red pixels occurring outside of the mapped LTZ areas, Fig. 3). The standard deviation is low (0.02–0.03) for the optimum threshold value from eight different Landsat scenes (covering seven years; 2003–2010). Therefore, there is confidence that this threshold of −0.53 has reasonable accuracy of classification without temporal variability significantly increasing uncertainty in the results.

The calibration of the SI values against field point data for mapping the MTZ indicated that a broad range of threshold values for identifying 'salt precipitation' pixels (i.e. MTZ) from 0.075 (increase in false negatives) to 0.124 (conservative, few false positives). Comparison of different thresholds against landform mapping of the MTZ at the calibration sites indicates that a threshold of 0.12 best delineates the MTZ (Fig. 3). This threshold falls on the conservative side of potential threshold ranges and would likely underestimate the spatial extent of salt precipitation on the surface, according to the producer accuracy. However, due to the thin salt crusting often observed, the pixel mixing effect may mean this is approximately the limit of the sensor in distinguishing salt crust from other high albedo materials. There is only a small amount

[1] For interpretation of color in Fig. 3, the reader is referred to the web version of this article.

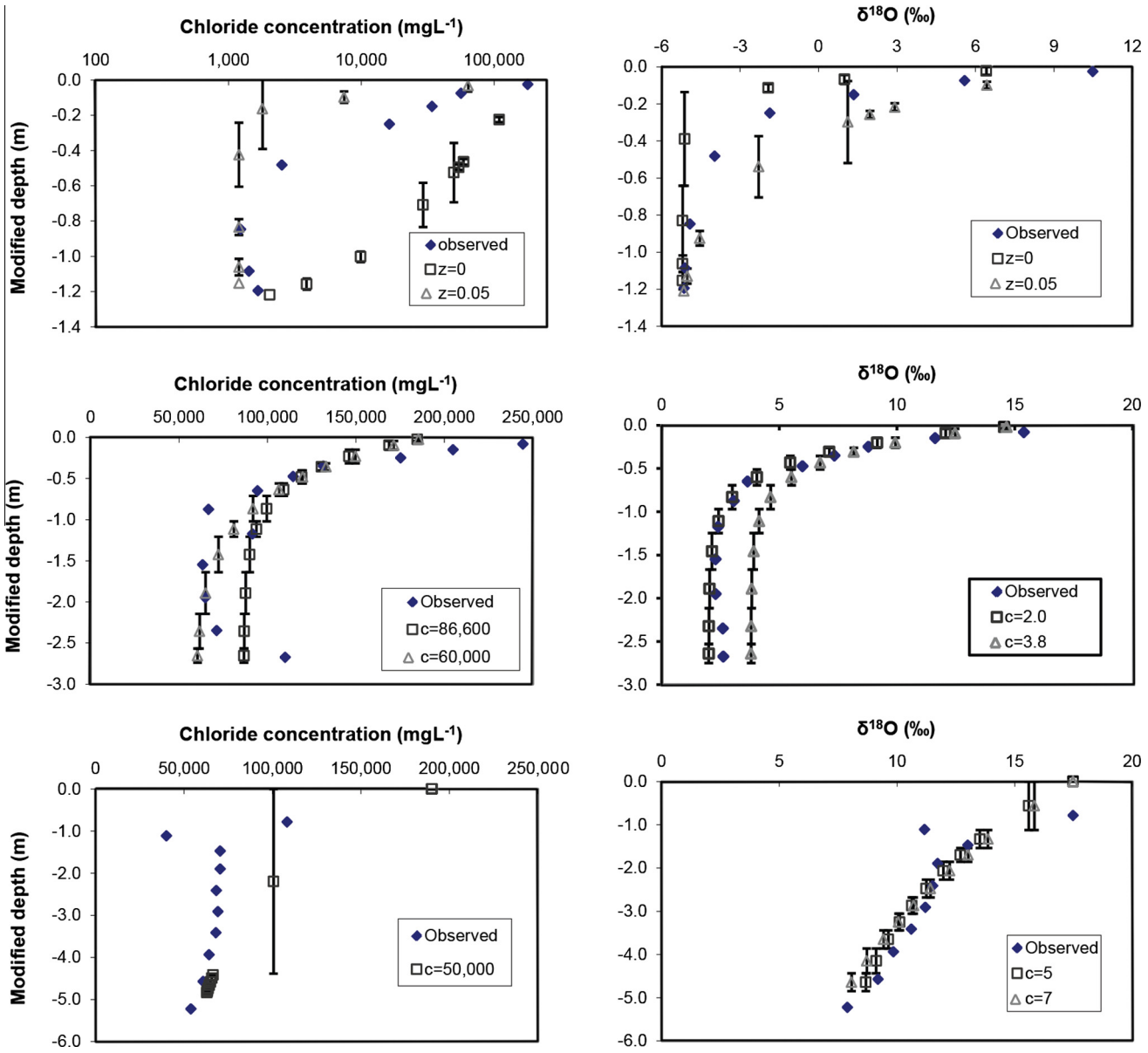

Fig. 6. Soil profile results from the LTZ (top – Elizabeth Springs; EL), MTZ (middle – Strangways Springs; ST in Fig. 1) and VTZ (bottom – Elizabeth Springs). Profiles compare observed tracer concentrations to modelled concentrations using the advection–diffusion model (Barnes and Allison, 1983), where '*z*' is the modelled position of the evaporation front and '*c*' is the modelled concentration of the unconfined groundwater. The 'modified depth' utilises the measured sample interval and its effective diffusion coefficient to transform the measured depths so that the whole profile can be represented by a single representative, average diffusion coefficient so that the modified total depth remains the same as the measured total depth (see Costelloe et al., 2014).

Table 2
Results for mapping of high discharge areas (LTZ, MTZ and carbonate) by supervised classification and landform mapping. Mapped areas are shown in km^2 in the upper rows and as a percentage of the total area for each discharge zone in the lower rows.

	Western area (km^2)		Mixing area (km^2)		Eastern area (km^2)		Total area (km^2)	
	Supervised	Landform	Supervised	Landform	Supervised	Landform	Supervised	Landform
LTZ	68.5	601.2	10.0	46.0	–	35.2	78.5	682.4
MTZ	34.0	353.5	4.3	84.4	7.3	24.4	45.6	462.3
Carbonate	20.8	11.3	–	7.6	0.5	–	21.3	18.9
	%	%	%	%	%	%	%	%
LTZ	87.3	88.1	12.7	6.8	–	5.2	100	100
MTZ	74.6	76.5	9.4	18.3	16.0	5.3	100	100
Carbonate	97.7	59.8	–	40.2	2.3	–	100	100

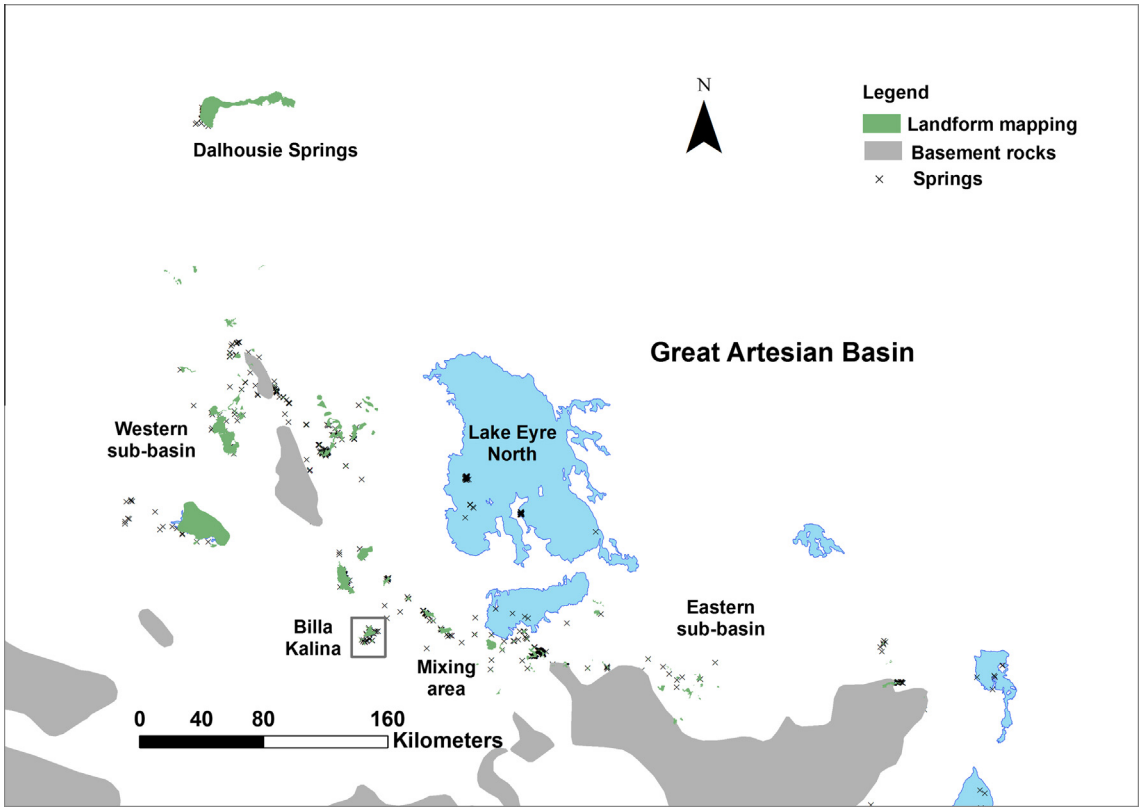

Fig. 7. Mapping of high discharge areas (LTZ and MTZ) using landform mapping over the south-western margin of the GAB. The distribution of artesian springs is shown for context. The supervised classification mapping is not shown as it is difficult to see at this scale but generally occurs within the areas of landform mapping. The Billa Kalina area (shown in greater detail in Fig. 8) is shown within the rectangle.

of spatial and temporal variability between the two calibration sites (mean SI of 0.12 at both sites and standard deviations of 0.01–0.014).

Comparing the supervised classification mapping to the landform mapping suggests that the former is significantly underestimating the area of the high discharge zones while the latter is possibly over-estimating the area (Table 2). Examination of the supervised classification mapping results at the site scale (e.g. BI, Fig. 8) illustrates the underestimation by this method. In particular, areas with patchy salt precipitation but a heavy stone lag, which field mapping and water table depth would place in the MTZ, are not identified at the spatial scale of the Landsat resolution. The more interpretative 'lumping' nature of the landform mapping captures the outer boundary of the high discharge zones but at the expense of ignoring smaller scale heterogeneity. The results of the two mapping techniques (Table 2) consistently show that the high discharge zones are most prevalent in the western sub-basin of the GAB. In contrast, the basin margins in the eastern sub-basin are characterised by a relative paucity of areas with high phreatic ET characteristics.

4.5. Regional scale flux estimates

The water balance for the GAB has previously been estimated by Habermehl (1980) and by steady-state and transient modelling at the whole-of-basin scale by the Bureau of Rural Sciences (BRS) (Welsh, 2000, 2006). In this study the steady-state GABFLOW model (Welsh, 2000) results are used in preference to the transient model results, as the latter treated vertical leakage as the water balance residual and was minimised during the model calibration (Welsh, 2006). The water balance for the South Australian portion of the GAB from the steady-state modelling is shown in Table 3 (reported in Arid Areas Catchment Water Management Board, 2004). The phreatic ET estimates from this study are compared to two key modelled water balance components; the estimate of total vertical leakage along the south-western margin of the GAB (100,010 ML y^{-1}) and the estimate of recharge from the western margin (59,495 ML y^{-1}).

Ranges of field-measured phreatic ET rates (Table 1) were estimated for LTZ, MTZ and carbonate discharge zones. The zones were separated into western and eastern sub-basins, reflecting groundwater inflow from the western and eastern margins of the GAB respectively, and a mixing zone that received inflow from both sub-basins. These provide the upper and lower bounds for use in simple up-scaling discharge estimates using the supervised classification and landform mapping of discharge areas. These bounds were then applied to the areas of each discharge zone using both mapping approaches (Table 2) and the estimated fluxes of phreatic ET for the study area were calculated, as shown in Table 4 and Fig. 9. The total modelled leakage (Table 3) provides a conceptual upper limit for comparison to the phreatic ET discharge while the modelled recharge from the western margin provides a conceptual upper limit to phreatic ET discharge within the western sub-basin.

Note that the VTZ zone was not included in this analysis and nor were any GAB discharge zones around mound springs in the large salt lakes (e.g. Eyre South, Blanche, Callabonna, Frome). In the large salt lakes it is not possible to separate out areas of GAB vertical leakage from evaporation of unconfined groundwater sourced from surface inflow recharge. Therefore, the flux estimates of Table 4 do not represent the entire GAB-sourced phreatic ET component in the field area but do indicate the main distribution of the areas of highest discharge. The higher (i.e. LTZ, MTZ, carbonate) phreatic zones mapped by supervised classification of satellite data account

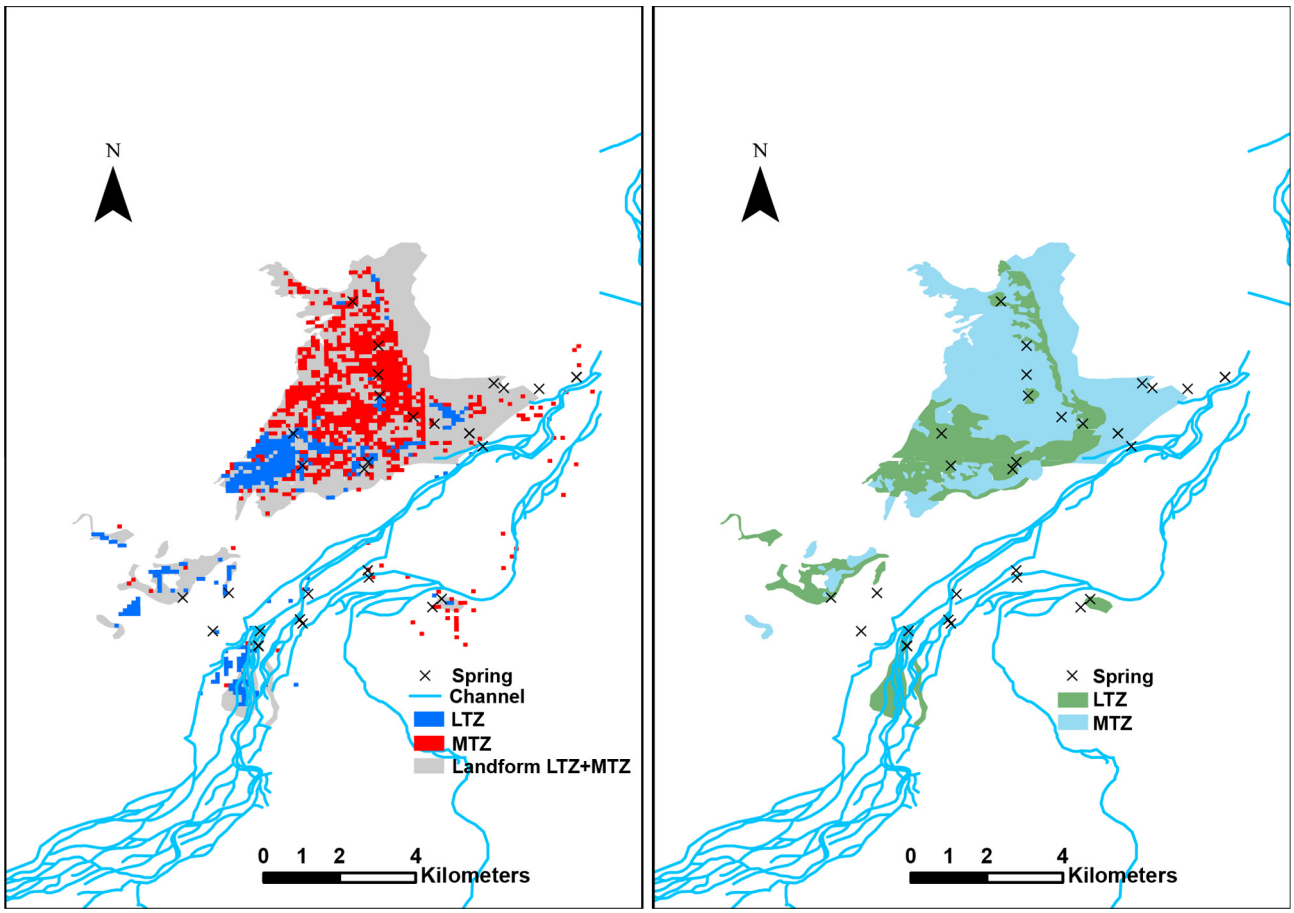

Fig. 8. Detail of Billa Kalina (BI in Fig. 1 and also shown in Fig. 7) discharge areas using supervised classification (left) and landform mapping (right). The supervised classification areas of high discharge (LTZ and MTZ) nearly always occur within the LTZ and MTZ identified by landform mapping.

Table 3
Summary of model flows (indicative) for the GAB within South Australia (AACWM Board, 2004; Welsh, 2000).

Water balance components	Inflow (ML y^{-1})	Outflow (ML y^{-1})
Horizontal flow (J-K aquifers)	58,400	1095
Bores	–	46,720
Springs	–	24,090
Recharge (western sub-basin)	59,495	–
Vertical leakage (from deeper Hutton Sandstone aquifer)	54,020	100,010
Sum	171,915	171,915

for 8–28% of the total vertical leakage component within South Australia estimated by BRS modelling (Table 4). Phreatic ET fed only from groundwater flowing from the western sub-basin are 7–24%, areas from the mixing zone are 1–3%, and areas from the eastern sub-basin are <1% of the model-estimated total vertical leakage for South Australia, respectively. The higher phreatic ET zones estimated by landform mapping account for 73–251% of the total vertical leakage component modelled by BRS (Table 4), with the western sub-basin being 64–216%, the mixing zone being 5–22% and the eastern sub-basin being 4–13% of the modelled total vertical leakage, respectively.

Table 4
Estimated phreatic ET fluxes for the south-western margin of the GAB using mapping of high discharge areas by supervised classification (Superv.) and landform (Landf.) mapping. The percentages are of the estimated flux relative to the total modelled vertical leakage flux for South Australia (see Table 3).

	Western area (ML y^{-1})		Mixing area (ML y^{-1})		Eastern area (ML y^{-1})		Total area (ML y^{-1})	
	Superv.	Landf.	Superv.	Landf.	Superv.	Landf.	Superv.	Landf.
LTZ	6851–20,553	60,121–180,362	1001–3004	4604–13,811	0	3519–10,556	7852–23,556	68,243–204,730
MTZ	340–3400	3535–35,348	43–433	844–8441	73–730	244–2443	456–4563	4623–46,232
Carb.	4–104	2–57	0	2–38	0–2	0	4–107	4–95
	%	%	%	%	%	%	%	%
LTZ	7–21	60–180	1–3	5–14	0	4–11	8–24	68–205
MTZ	0–3	4–35	<1	1–8	0–1	0–2	1–5	5–46
Carb.	0	0	0	0	0	0	0	0

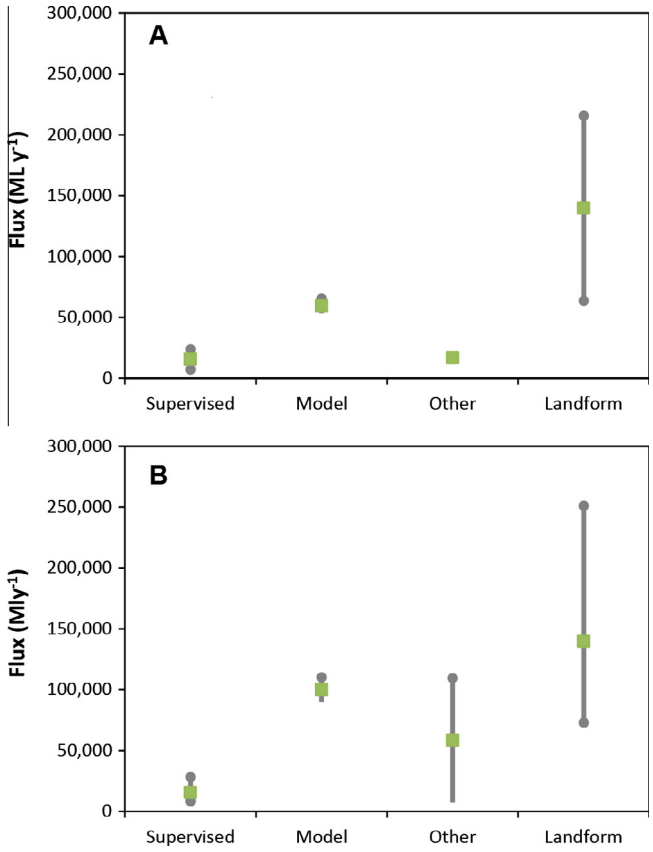

Fig. 9. Comparison of phreatic ET flux estimates, up-scaled using supervised classification ('Supervised') and landform mapping ('Landform'), to steady state modelling ('Model', Table 3) and comparable ('Other', Fulton, 2012; Love et al., 2013b) estimates of western sub-basin recharge (A) and total vertical leakage (B). The phreatic ET estimates show the median and range while the steady state modelled value has been given an arbitrary range of ±10%. Note that the Fulton (2012) estimate of western sub-basin recharge only includes fluvial recharge from the north-western rivers and represents a probable minimum value, while the total vertical leakage estimate of Love et al. (2013b) is from noble gas analysis of unconfined groundwater around the south-western margin of the GAB.

5. Discussion

5.1. Uncertainties in estimates of phreatic ET

There are three main groups of uncertainties associated with the results from this study: uncertainties in flux estimates, uncertainties in mapping of discharge zones, and uncertainties in the assumptions of the methods.

The field measured flux rates for the different discharge zones (Table 1) show high variability within and across the three measurement techniques but with considerable overlap. The measured phreatic ET rates are larger than the range identified by Woods (1990) using soil profile modelling around the Lake Eyre Spring supergroup (Table 1), recognizing that those results were more focused on data collected in what we map as the MTZ and VTZ zones. The VTZ phreatic evaporation rates shown in Table 1 are considerably larger than diffusive leakage rates through the aquitard, measured by Harrington et al. (2013) from deep profiles distal to the main discharge zones, and these distal areas are equivalent to the ZDZ of Fig. 2. The higher rates identified in this project for the LTZ and MTZ zones were consistent with results from arid zone environments with shallow water tables (e.g. Allison and Barnes, 1985; Tyler et al., 1997) where phreatic evaporation rates of 100s mm y^{-1} have been measured (Table 1). The LTZ in the study region typically only had a very thin salt crust of 1–3 mm, which is likely to due to periodic wetting of the soil surface layer and removal of salt by rainfall. Thus it lacked the thick, dry salt crust that has been found to result in very low phreatic evaporation rates reported for some salt lakes with thick crusts (e.g. Salar de Atacama; Kampf et al., 2005). The upper range of the field measured rates only represents approximately 40% of the areal potential evapotranspiration rate estimated for this region (Australian Bureau of Meteorology) and so these rates still represent likely water-limited conditions, although the elevated salinity of the near surface soil water will also limit ET rates. Some of the higher measured rates were affected by rainfall and so do not represent 'steady-state' phreatic ET. However, even the rain-affected results lay within the range defined by the other measurements of phreatic ET and so may represent the upper limit of bare soil evaporation supported by capillary rise through the soil. The measured fluxes also generally decrease with increases in the depth to water table, consistent with analytical and experimental studies (Gardner, 1958; Gowing et al., 2006). This was best illustrated in the upper ranges of fluxes estimated from the soil profile modelling as the microlysimeter data appeared to be more sensitive to local-scale factors (Table 1).

The role of phreatic transpiration in the ET flux has not been explicitly considered in this study. Halophytic shrubs are relatively sparse in the field area and largely restricted to the LTZ and MTZ zones, with the VTZ generally containing very little vegetation cover. The results in Table 1 show a similarity in range between the microlysimeter results, measuring bare soil evaporation, and eddy covariance results, measuring total above-ground ET flux, for both the LTZ and MTZ. This indicates that the selected range of phreatic ET fluxes encompasses the likely contribution of phreatic transpiration. Trees are confined to the drainage lines and, though in close spatial proximity to the discharge zones at a number of sites, these are largely excluded from the supervised classification and landform mapping of discharge areas due to the influence of fluvial recharge on the unconfined groundwater (Costelloe et al., 2012). As a result, unaccounted for phreatic ET from phreatophytic trees is not considered to be a significant contributor to the GAB water balance.

The two forms of mapping high discharge zones (landform mapping and supervised classification) are interpreted as providing effective upper and lower bounds to estimation of the different phreatic ET zones. This is illustrated in Fig. 9 where the estimates for the entire south-western margin are compared to the steady state numerical model total leakage flux (Fig. 9a) and the estimates for the western sub-basin are compared to the modelled recharge flux for the western margin of the GAB (Fig. 9b). The steady state modelled fluxes also have high uncertainty but provide an independent measure for comparison against the results of this study, and other independent estimates of GAB diffuse discharge (Love et al., 2013b) and western margin recharge (Fulton, 2012). In both cases, the steady state modelling fluxes (specified in Table 3) are greater than the supervised classification estimates but overlap, or are less than the landform estimates. The landform mapping is more of an interpretative 'lumping' exercise as it identifies an envelope around characteristic discharge areas and so will not account for small scale landform heterogeneity, particularly caused by micro-topographic, vegetation and soil variations. In contrast, the supervised classification of the Landsat data is significantly affected by pixel mixing effects due to its spatial resolution (30 m pixel size) and is unable to distinguish between areas with heterogeneous mixtures of discharge and non-discharge surface characteristics (e.g. salt precipitates and stone lags). Nevertheless, both methods show similar spatial distributions of high discharge zones, albeit with significant differences in the mapped area at any specific location but with the landform mapping nearly always encompassing the areas mapped by supervised classification. The

landform mapping will also incorporate areas with halophytic vegetation in the LTZ and MTZ that account for the transpiration component of phreatic ET, and which may not be mapped using the supervised classification.

The major assumption of using phreatic ET rates to measure artesian leakage is that the unconfined groundwater is dominantly sourced from artesian leakage, rather than meteoric recharge. Within the field area, hydrogeochemical modelling showed that the composition of the shallow unconfined groundwater was consistent with evapoconcentration of the underlying artesian groundwater at a number of sites, but that other sites within the field area, particularly discharge zones near surface streams, showed evidence of significant contributions from meteoric recharge (Costelloe et al., 2012). Results from another study, which sampled noble gases from the unconfined groundwater from parts of the field area, were also consistent with GAB discharge along preferential flow paths being the dominant source of unconfined groundwater around the spring groups (Love et al., 2013b). The noble gas analysis estimates of Love et al. (2013b) were 7300–109,500 ML y^{-1}, and consistent with the range of phreatic ET estimates from this study (Table 4). The sites with significant meteoric recharge were located close to lower order streams and also showed piezometric responses to flow events, indicating that recharge was due to fluvial processes (Costelloe et al., 2012). The lack of a significant pluvial recharge signal in the GAB discharge zones is also consistent with most of the soil profiles showing long-term phreatic evaporation characteristics (Costelloe et al., 2014). Woods (1990) also found that most soil profiles collected in the area near Lake Eyre South were consistent with long-term phreatic evaporation. Nevertheless, the occurrence of fluvial recharge and the spatial correlation between many GAB discharge zones and drainage systems in the low-lying parts of the landscape means that the phreatic ET fluxes estimated from this study represent a conceptual upper bound to GAB vertical leakage from the mapped areas.

5.2. Hydrogeological implications of flux estimates

Despite the large uncertainties associated with the field estimates of phreatic ET (Table 1) and the mapping of discharge areas (Table 2), the results provide important constraints on the upward leakage loss term from the GAB and its spatial distribution. Note that the flux estimates in Table 4 do not include spring flow, discharge into large salt lakes or discharge from the VTZ surrounding the LTZ and MTZ areas.

In the western sub-basin (Table 4), much of the estimated recharge can be accounted for by phreatic ET in the LTZ and MTZ areas located around the spring groups occurring close to the Basin margins. The results imply that vertical leakage rates distal to the margins are very low, and/or the inflow to this part of the GAB is currently underestimated. This finding concurs with the very low hydraulic conductivities (e.g. $<1 \times 10^{-12}$ ms^{-1}) and discharge rates estimated for the Bulldog Shale aquitard in the region of the south-western GAB discharge area using hydrogeochemical analysis of porewater and modelling (Harrington et al., 2013). In effect, unfaulted thick sequences of the Bulldog Shale aquitard experience effectively zero discharge at an annual time scale.

The likelihood that the steady-state numerical modelling (see Table 3) has underestimated inflow (i.e. recharge) to the western sub-basin is low. Other field studies have found low recharge rates and long residence times in the unsaturated zone (1000s years) indicating that recharge is not in steady state with discharge (i.e. recharge < discharge), and that current discharge likely represents recharge from wetter periods, with effectively zero recharge under current climate conditions. For example, the diffuse recharge through outcropping aquifer rocks along the western margin of the GAB has been estimated using chloride mass balance at a mean annual rate 0.15 mm y^{-1} (range 0.01–1.8 mm y^{-1}) and deep unsaturated soil profile analysis at 0.34 ± 0.11–1.65 ± 0.42 mm y^{-1} (Love et al., 2000, 2013a). Recharge to the western sub-basin is likely to be dominated by fluvial recharge from ephemeral rivers crossing the north-western margin of the GAB that supplies flow paths to the high discharging Dalhousie Springs complex. The spring discharge from the Dalhousie Springs Complex is estimated to be approximately 21,000 ML y^{-1} (Habermehl, 1982), but current fluvial recharge from the north-western rivers is estimated at only 17,000 ML y^{-1} based on analytical modelling of observed recharge events (Fulton, 2012). The area of high discharge zones measured by both landform mapping and supervised classification was dominated by Dalhousie Springs (i.e. 43.3% of total LTZ and 9.8% of total MTZ), although these areas include probable re-infiltration of spring outflow that may make a significant contribution to the definition of the phreatic ET zones. However, these figures indicate that the vertical leakage flux for the Dalhousie Springs is in the range of 3400–93,200 ML y^{-1}, in addition to the spring discharge of approximately 21,000 ML y^{-1}, emphasising that even in this area with relatively high current fluvial recharge, the water balance is not in steady state.

In contrast to the interpreted water balance of the western sub-basin, the results for the eastern sub-basin suggest that vertical leakage rates around the Basin margin are very low and therefore, more of the vertical leakage component in the eastern sub-basin is occurring distal to the Basin margins. For instance, of the 112,000 ML y^{-1} estimated inflow to South Australia from the eastern GAB (Table 3), the phreatic ET component for the eastern and mixing sub-basins only comes to a maximum of approximately 35,000 ML y^{-1}. These results suggest that pathways for vertical leakage are likely to be more complex (i.e. more faulting allowing preferential leakage) from the deeper eastern sub-basin than for the shallow western sub-basin and allow more leakage distal to the GAB margins. For instance, overlying non-artesian aquifers could be capturing much of the vertical leakage from the artesian basal aquifers and control the spatial distribution of the ultimate destination of the leaked groundwater. Alternatively, some of the unaccounted for loss could be GAB contribution to phreatic ET from large salt lakes, such as Lake Eyre and Lake Frome.

Our results indicate that groundwater models for the GAB need to consider spatially explicit areas of high discharge that are associated with the spring complexes. The close proximity of the springs and high discharge zones suggests that the concept of harvesting the vertical leakage component (Sultan et al., 2007) would not improve the sustainability of water extraction (i.e. in terms of limiting effects on high value spring ecosystems) as the preferential flow pathways for springs and leakage are likely to be closely linked.

6. Conclusions

This research has demonstrated that phreatic ET from leakage zones to the unconfined water table around artesian spring groups makes up a significant component of the water balance of the GAB. The highest recorded rates are consistent with those recorded at groundwater discharge playa environments and typically decrease as the depth to the water table increases away from the active springs. The results provide insights into the spatial distribution of the phreatic ET loss term and overall functioning of the GAB. In the western sub-basin, the results indicate that most of the discharge flux from the GAB occurs in the LTZ and MTZ areas surrounding spring groups, and is also consistent with other studies indicating that discharge currently exceeds recharge along the western margin of the GAB. In the eastern sub-basin, most of the discharge flux must be occurring away from the spring groups

located on the GAB south-western margin. The integration of field-based estimates of phreatic ET with a conceptual framework for mapping discharge zones provides a robust method for constraining important discharge components of a large, arid zone, groundwater system.

Acknowledgments

Funding for this research was provided by Australian Research Council Linkage grant LP0774814, in conjunction with industry partners BHP-Billiton, Great Artesian Basin Coordinating Committee, Santos Limited and the South Australian Arid Lands Natural Resource Management Board. The permission of the following landholders to conduct fieldwork is gratefully acknowledged; Robert Khan (Marree Station), George Morphett (Callanna Station), David Brook and Frank Booth (Murnpeowie Station), Reg Dodd (Finniss Springs Station), Bobby Hunter (Stuart Creek Station), Randall Crozier (Mt Anna Station), and Trevor Williams (Nilpinna Station). The fieldwork would not have been possible without the assistance of Graeme Tomlinson, Dinh Phu Nguyen, Belis Matabire, Maria Friderich, Peter Richards, Susan Hayes and Richard Evans. We thank three anonymous reviewers for their insightful and constructive reviews that helped improve this paper.

Appendix A. Supplementary material

Supplementary data associated with this article can be found, in the online version, at http://dx.doi.org/10.1016/j.jhydrol.2015.09.026.

References

Allison, G.B., Barnes, C.J., 1985. Estimation of evaporation from the normally "dry" Lake Frome in South Australia. J. Hydrol. 78, 229–242.

Arid Areas Catchment Water Management Board, 2004. Water Allocation Plan: Far North Prescribed Wells Area. Arid Areas Catchment Water Management Board, Adelaide. <http://www.naturalresources.sa.gov.au/aridlands/water/water-allocation-plan> (last accessed 14.04.15).

Barnes, C.J., Allison, G.B., 1983. The distribution of deuterium and ^{18}O in dry soils, 1. Theory J. Hydrol. 60, 141–156.

Becker, M.W., 2006. Potential for satellite remote sensing of ground water. Ground Water 44, 306–318.

Boast, C.W., Robinson, T.M., 1982. A 'micro-lysimeter' method for determining evaporation from bare soil: description and laboratory evaluation. Soil Sci. Soc. Am. J. 46, 689–696.

Bredehoeft, J.D., Papadopulus, S.S., Cooper Jr., H.H., 1982. Groundwater: the Water Budget Myth in Scientific Basis of Water Resource Management. National Research Council Geophysics Study Committee, National Academy Press, Washington, DC, pp. 51–57.

Brunner, P., Hendricks Franssen, H.J., Kgotlhang, L., Bauer-Gottwein, P., Kinzelback, W., 2007. How can remote sensing contribute in groundwater modelling? Hydrogeol. J. 15, 5–18.

Brunner, P., Li, H.T., Kinzelback, W., Li, W.P., Dong, X.G., 2008. Extracting phreatic evaporation from remotely sensed maps of evapotranspiration. Water Resour. Res. 44, W08428. http://dx.doi.org/10.1029/2007WR006063.

Brunner, P., Doherty, J., Simmons, C.T., 2012. Uncertainty assessment and implications for data acquisition in support of integrated hydrologic models. Water Resour. Res. 48, W07513. http://dx.doi.org/10.1029/2011WR011342.

Congalton, R.G., 1991. A review of assessing the accuracy of classifications of remotely sensed data. Remote Sens. Environ. 37, 35–46.

Costelloe, J.F., Matic, V., Western, A.W., 2009. Using microlysimeters to estimate evaporation in arid zone, groundwater discharge environments. In: H2009: 32nd Hydrology and Water Resources Symposium, Newcastle: Adapting to Change. Barton, A.C.T.: Engineers Australia, 2009, pp. 1397–1406.

Costelloe, J.F., Irvine, E.C., Western, A.W., Tyler, M., 2012. Identifying fluvial recharge and artesian upwards leakage contributions to arid zone shallow, unconfined groundwater. Chem. Geol. 326–327, 189–200.

Costelloe, J.F., Irvine, E.C., Western, A.W., 2014. Uncertainties around modelling of steady-state phreatic evaporation with field soil profiles of ^{18}O and chloride. J. Hydrol. 511, 229–241.

Danielopol, D.L., Griebler, C., Gunatilaka, A., Notenboom, J., 2003. Present state and future prospects for groundwater ecosystems. Environ. Conserv. 30, 104–130.

Famiglietti, J.S., Lo, M., Ho, S.L., Bethune, J., Anderson, K.J., Syed, H., Swenson, S.C., de Linage, C.R., Rodell, M., 2011. Satellites measure recent rates of groundwater depletion in California's Central Valley. Geophys. Res. Lett. 38, L03403. http://dx.doi.org/10.1029/2010GL046442.

Famiglietti, J.S., 2014. The global groundwater crisis. Nat. Clim. Change 4, 945–948.

Fensham, R.J., Price, R.J., 2004. Ranking spring wetlands in the Great Artesian Basin of Australia using endemicity and isolation of plant species. Biol. Conserv. 119, 41–50.

Fulton, S.A., 2012. Technical Report Great Artesian Basin Resource Assessment. Department of Land Resource Management, Report 14/2012A, Darwin, October 2012.

Gardner, W.R., 1958. Some steady-state solutions of the unsaturated moisture flow equation with applications to evaporation from a water table. Soil Sci. 85, 228–332.

Gowing, J.W., Konukcu, F., Rose, D.A., 2006. Evaporative flux from a shallow water table: the influence of a vapour–liquid phase transition. J. Hydrol. 321, 77–89.

Habermehl, M.A., 1980. The Great Artesian Basin, Australia. BMR J. Aust. Geol. Geophys. 5, 9–38.

Habermehl, M.A., 1982. Springs in the Great Artesian Basin, Australia – their origin and nature. BMR J. Aust. Geol. Geophys. 235, 1–50.

Harrington, G.A., Gardner, W.P., Smerdon, B.D., Hendry, M.J., 2013. Palaeohydrogeological insights from natural tracer profiles in aquitard porewater, Great Artesian Basin, Australia. Water Resour. Res. 49, 4054–4070. http://dx.doi.org/10.1002/wrcr.20327.

Harvey, F.E., Ayers, J.F., Gosselin, D.C., 2007. Ground water dependence of endangered ecosystems: Nebraska's eastern saline wetlands. Ground Water 45, 736–752. http://dx.doi.org/10.1111/j.1745-6584.2007.00371.x.

Hendricks Franssen, H.J., Brunner, P., Makobo, P., Kinzelbach, W., 2008. Equally likely inverse solutions to a groundwater flow problem including pattern information from remote sensing images. Water Resour. Res. 44, W01419. http://dx.doi.org/10.1029/2007WR006097.

Herczeg, A.L., Torgersen, T., Chivas, A.R., Habermehl, M.A., 1991. Geochemistry of ground waters from the Great Artesian Basin Australia. J. Hydrol. 126, 225–245.

Kalf, F.R.P., Woolley, D.R., 2005. Applicability and methodology of determining sustainable yield in groundwater systems. Hydrogeol. J. 13, 295–312.

Kampf, S.K., Tyler, S.W., Ortiz, C.A., Muñoz, J.F., Adkins, P.L., 2005. Evaporation and land surface energy budget at the Salar de Atacama, Northern Chile. J. Hydrol. 310, 236–252.

Kampf, S.K., Tyler, S.W., 2006. Spatial characterisation of land surface energy fluxes and uncertainty information at the Salar de Atacama, Northern Chile. Adv. Water Resour. 29, 336–354.

Keppel, M.N., Clarke, J.D.A., Halihan, T., Love, A.J., Werner, A.D., 2011. Mound springs in the arid Lake Eyre South region of South Australia: a new depositional tufa model and its controls. Sediment. Geol. 240, 55–70.

Leblanc, M., Favreau, G., Tweed, S., Leduc, C., Razack, M., Mofor, L., 2007. Remote sensing for groundwater modelling in large semiarid areas: Lake Chad Basin, Africa. Hydrogeol. J. 15, 97–100.

Love, A.J., Herczeg, A.L., Sampson, L., Cresswell, R.G., Fifield, L.K., 2000. Sources of chloride and implications for ^{36}Cl dating of old groundwater, southwestern Great Artesian Basin, Australia. Water Resour. Res. 36, 1561–1574.

Love, A.J., Wohling, D., Fulton, S., Rousseau-Gueutin, P., De Ritter, S., 2013a. Allocating Water and Maintaining Springs in the Great Artesian Basin, Volume II: Groundwater Recharge. Hydrodynamics and Hydrochemistry of the Western Great Artesian Basin, National Water Commission, Canberra.

Love, A.J., Shand, P., Crossey, L., Harrington, G.A., Rousseau-Gueutin, P., 2013b. Allocating Water and Maintaining Springs in the Great Artesian Basin, Volume III: Groundwater Discharge of the Western Great Artesian Basin, National Water Commission, Canberra.

Merlin, O., Walker, J., Panciera, R., Young, R., Kalma, J., Kim, E., 2007. Soil moisture measurement in heterogenous terrain. In: Oxley, L., Kulasiri, D. (Eds.), MODSIM 2007 International Congress on Modelling and Simulation, Modelling and Simulation Society of Australia and New Zealand, December 2007, pp. 2604–2610. <http://www.mssanz.org.au/MODSIM07/papers/46_s60/SoilMoistures60_Merlin_.pdf>.

Mudd, G.M., 2000. Mound springs of the Great Artesian Basin in South Australia: a case study from Olympic Dam. Environ. Geol. 39, 463–476.

Patten, D.T., Rouse, L., Stromberg, J.C., 2008. Isolated spring wetlands in the Great Basin and Mojave Deserts, USA: potential responses of vegetation to groundwater withdrawal. Environ. Manage. 41, 398–413.

Plauborg, F., 1995. Evaporation from bare soil in a temperate humid climate – measurement using micro-lysimeters and time domain reflectometry. Agr. For. Meteorol. 76, 1–17.

Rodell, M., Velicogna, I., Famiglietti, J.S., 2009. Satellite-based estimates of groundwater depletion in India. Nature 460, 999–1002. http://dx.doi.org/10.1038/nature08238.

Sanderson, J.S., Cooper, D.J., 2008. Ground water discharge by evapotranspiration in wetlands of an arid intermountain basin. J. Hydrol. 351, 344–359.

Shanafield, M., Cook, P.G., Gutiérrez-Jurado, H.A., Faux, R., Cleverly, J., Eamus, D., 2015. Field comparison of methods for estimating groundwater discharge by evaporation and evapotranspiration in an arid-zone playa. J. Hydrol. 527, 1073–1083.

Stisen, S., Sonnenborg, T.O., Højberg, A.L., Troldborg, L., Refsgaard, J.C., 2010. Evaluation of climate input biases and water balance issues using a coupled surface – subsurface model. Vadose Zone J. 10, 37–53. http://dx.doi.org/10.2136/vzj2010.0001.

Sultan, M., Yan, E., Sturchio, N., Wagdy, A., Abdel Gelil, K., Becker, R., Manocha, N., Milewski, A., 2007. Natural discharge: a key to sustainable utilization of fossil groundwater. J. Hydrol. 335, 25–36.

Tripathi, N.K., Rai, B.K., Dwivedi, P., 1997. Spatial modelling of soil alkalinity in GIS environment using IRS data. Paper presented at the 18th Asian Conference in

Remote Sensing, Kuala Lumpur, October 1997. <http://geospatialworld.net/Paper/Application/ArticleView.aspx?aid=285> (last accessed 24.06.15).
Tyler, S.W., Kranz, S., Parlange, M.B., Albertson, J., Katul, G.G., Cochran, G.F., Lyles, B. A., Holder, G., 1997. Estimation of groundwater evaporation and salt flux from Owens Lake, California, USA. J. Hydrol. 200, 110–135.
Tyler, S.W., Muñoz, J.F., Wood, W.W., 2006. The response of playa and Sabkha hydraulics and mineralogy to climate forcing. Ground Water 44, 329–338.
van Dijk, A.I.J., Renzullo, L.J., Rodell, M., 2011. Use of Gravity Recovery and Climate Experiment terrestrial water storage retrievals to evaluate model estimates by the Australian water resources assessment system. Water Resour. Res. 47, W11524. http://dx.doi.org/10.1029/2011WR010714.
Wada, Y., van Beek, L.P.H., van Kempen, C.M., Reckman, J.W.T., Vasak, S., Bierkens, M.F.P., 2010. Global depletion of groundwater resources. Geophys. Res. Lett. 37, L20402. http://dx.doi.org/10.1029/2010GL044571.
Wang, H., Guan, H., Gutiérrez-Jurado, H.A., Simmons, C.T., 2014. Examination of water budget using satellite products over Australia. J. Hydrol. 511, 546–554.
Welsh, W.D., 2000. GABFLOW: A Steady State Groundwater Flow Model of the Great Artesian Basin. Bureau of Rural Sciences, Canberra.
Welsh, W.D., 2006. Great Artesian Basin Transient Groundwater Model. Bureau of Rural Sciences, Canberra.
Woods, P.H., 1990. Evaporative Discharge of Groundwater from the Margin of the Great Artesian Basin, Near Lake Eyre, South Australia. PhD Thesis, Flinders University, Australia.
Xu, H., 2006. Modification of normalised difference water index (NDWI) to enhance open water features in remotely sensed imagery. Int. J. Remote Sens. 27 (14), 3025–3033.